JOC Article
pubs.acs.org/joc

Phospha-Münchnones: Electronic Structures and 1,3-Dipolar Cycloadditions

Daniel J. St-Cyr,[†] Marie S. T. Morin,[†] Francine Bélanger-Gariépy,[‡] Bruce A. Arndtsen,*[,†] Elizabeth H. Krenske,[§] and K. N. Houk*[,§]

[†]*Department of Chemistry, McGill University, 801 Sherbrooke Street West, Montreal, Quebec H3A 2K6, Canada,* [‡]*Département de Chimie, Université de Montréal, 2900, Boulevard Édouard-Montpetit, Montréal, Québec H3T 1J4, Canada, and* [§]*Department of Chemistry and Biochemistry, University of California, Los Angeles, California 90095*

bruce.arndtsen@mcgill.ca; houk@chem.ucla.edu

Received May 2, 2010

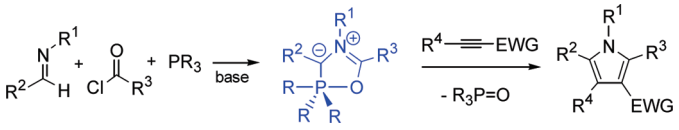

The reaction of imines, acid chlorides, PR_3, and base generates a new class of 1,3-dipoles: phospha-Münchnones. These 1,3-dipoles can undergo cycloadditions with alkynes followed by loss of phosphine oxides to form pyrroles. Cycloaddition reactivity is dependent upon the PR_3 employed, with PhP(catechyl) (catechyl = *o*-$O_2C_6H_4$) providing the most rapid cycloadditions and optimal pyrrole yields. ^1H, ^{13}C, and ^{31}P NMR analysis and computations indicate that electron-poor catechyl-substituted phosphonites and phosphites favor a cyclic 1,3-dipolar structure, while more electron-rich phosphines instead favor the valence tautomeric acyclic ylides. X-ray crystallographic studies confirm this. Density functional theory calculations support the wide variety of P−O interactions induced by different PR_3 groups and indicate that the most efficient concerted 1,3-dipolar cycloadditions are those for dipoles whose ground-state geometry is most like the transition-state geometry. Reactions of these dipoles with monosubstituted alkynes bearing an electron-withdrawing group are calculated to occur by stepwise mechanisms. The presence of the phosphorus unit creates a large electronic bias across the 1,3-dipole, allowing for regioselective cycloadditions with substituted alkynes.

Introduction

1,3-Dipolar cycloaddition is a versatile route to five-membered heterocycles. An impressive array of 1,3-dipoles have emerged over the past several decades, including such well-known substrates as nitrones, azomethine ylides, nitrile ylides, substituted azides, Sydnones, and Münchnones.[1−4] While certain 1,3-dipoles are relatively easily generated (e.g., substituted azides), many others require a multistep synthesis to assemble the precursors, followed by the use of reactive reagents to create the dipole.[1] This not only adds further steps to the overall synthesis but also makes substrate variation difficult to achieve.

One example of the latter type of dipoles is Münchnones, or 1,3-oxazolium 5-oxides (**1**), which were first reported by Huisgen in 1964.[3,4] Münchnones typically extrude CO_2 upon cycloaddition with alkynes, leading to pyrroles. This reactivity has been exploited in the synthesis of biologically relevant pyrroles,[5] pyrrolines,[5,6] imidazoles,[7] and imidazolines.[8]

(1) (a) *The Chemistry of Heterocyclic Compounds: Synthetic Applications of 1,3-Dipolar Cycloaddition Chemistry Toward Heterocycles and Natural Products*; Padwa, A., Pearson, H., Eds.; Wiley: New York, 2002; Vol. 45. (b) *1,3-Dipolar Cycloaddition Chemistry*; Padwa, A., Ed.; Wiley: New York, 1984.

(2) (a) Stewart, F.; H., C. *Chem. Rev.* **1964**, *64*, 129. (b) Lewis, W. G.; Green, L. G.; Grynszpan, F.; Radic, Z.; Carlier, P. R.; Taylor, P.; Finn, M. G.; Sharpless, K. B. *Angew. Chem., Int. Ed.* **2002**, *41*, 1053.

(3) Lawson, A.; Miles, D. H. *Chem. Ind.* (*London*) **1958**, 461.

(4) (a) Huisgen, H.; Gotthardt, H.; Bayer, H. O. *Angew. Chem., Int. Ed. Engl.* **1964**, *3*, 135. (b) Huisgen, H.; Gotthardt, H.; Bayer, H. O.; Schaefer, F. C. *Angew. Chem., Int. Ed. Engl.* **1964**, *3*, 136.

(5) (a) For reviews of Münchnones, see: Gribble, G. W. In *Oxazoles: Synthesis, Reactions, and Spectroscopy, A*; Palmer, D. C., Ed.; Wiley: New York, 2003; Vol. 60, Chapter 4. (b) Gingrich, H. L.; Baum, J. S. In *Oxazoles, The Chemistry of Heterocyclic Compounds*; Turchi, I. J., Ed.; Wiley: New York, 1986; Vol. 45, Chapter 4.

(6) For examples: (a) Melhado, A. D.; Luparia, M.; Toste, F. D. *J. Am. Chem. Soc.* **2007**, *129*, 12638. (b) Bélanger, G.; April, M.; Dauphin, E.; Roy, S. *J. Org. Chem.* **2007**, *72*, 1104. (c) Peddibhotla, S.; Tepe, J. J. *J. Am. Chem. Soc.* **2004**, *126*, 12776.

(7) For examples, see: (a) Croce, P. D.; Rerraccioli, R.; La Rosa, C. *Tetrahedron* **1999**, *55*, 201. (b) Siamaki, A. R.; Arndtsen, B. A. *J. Am. Chem. Soc.* **2006**, *128*, 6050.

(8) (a) Dghaym, R. D.; Dhawan, R.; Arndtsen, B. A. *Angew. Chem., Int. Ed.* **2001**, *40*, 3228. (b) Fisk, J. A.; Mosey, R. A.; Tepe, J. J. *Chem. Soc. Rev.* **2007**, *36*, 1432.

DOI: 10.1021/jo1008383 Published on Web 05/18/2010

SCHEME 1. Generation and Cycloaddition of 2[12]

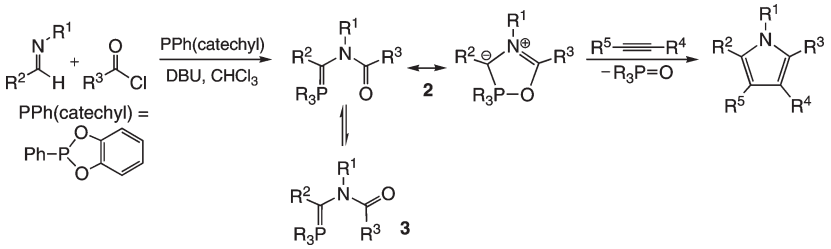

Münchnones are most commonly generated via the dehydration of the corresponding α-amido acids,[4,5,9] and multistep syntheses are required if these precursors derive from non-natural amino acids. In addition, cycloaddition of Münchnones with unsymmetrical substrates (e.g., unsymmetrical alkynes or alkenes) often leads to a mixture of regioisomeric products, unless there is a large steric or electronic bias between R^2 and R^3.[5,10] The regioisomers can be difficult to separate, and yields are limited.

We recently reported a one-pot synthesis of Münchnones that involves the palladium-catalyzed coupling of imines, acid chlorides, and carbon monoxide.[11] This procedure enables various Münchnone-derived products to be constructed in a modular fashion, where the $R^2C-N(R^1)-CR^3$ unit arises from the imine and acid chloride fragments. The synthesis is efficient, but the scope of products can be limited (particularly when employing unstable reagents such as enolizable imines, *C*- or *N*-functionalized imines, or α-acidic acid chlorides), and cycloadditions with unsymmetrical dipolarophiles still result in a mixture of regioisomeric products.

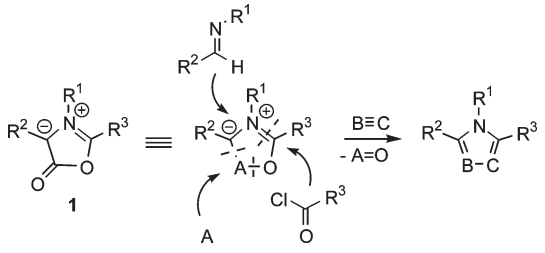

FIGURE 1. Modular design of Münchnone analogues.

We discovered that a synthetic equivalent to Münchnones can be generated when the carbonyl fragment in **1** (A = CO, Figure 1) is replaced with an R_3P unit (**2**, Scheme 1).[12] The phospha-Münchnones **2** have also been called Montréalones.[13] Dipole **2** is the valence tautomer of an amido-substituted phosphorus ylide in circumstances where the ylide adopts a suitable conformation to enable P−O interaction. Compound **2** is represented as a resonance hybrid, but separate, valence tautomeric structures are conceivable. For example, conformations where there is no potential for cyclic P−O interaction (such as **3**) can only be phosphorus ylides, while **2** could be a blend of phosphorus ylide and 1,3-dipolar azomethine ylide. Consistent with the latter structure, catechyl-substituted phosphonites undergo a multicomponent coupling with imines and acid chlorides to generate **2**, which reacts with alkynes to yield pyrroles in analogy to Münchnones. The new compounds **2** have also been characterized theoretically.[13]

We now report a detailed study of these new 1,3-dipoles and their transformations. This includes the observation that the structure, and 1,3-dipolar cycloaddition reactivity, are very sensitive to the nature of the PR_3 group. X-ray structural analysis has allowed the full characterization of a cyclic dipole, **2b**, obtained from the catechyl-containing phosphonite PhP(*o*-$O_2C_6H_4$) (PhP(catechyl)), as well as an acyclic ylide, **3a**, obtained from PPh_3. Density functional theory calculations provide explanations of the effects of P-substituents on dipole structure and reactivity. We also examine the mechanisms, scope, and selectivities of the cycloadditions of **2** and their application to the regioselective synthesis of diversely substituted pyrroles.

Results and Discussion

I. Influence of PR_3 on Cycloaddition Reactivity. As we have previously communicated,[12] compounds **2**/**3** can be generated by the in situ reaction of imines with acid chlorides, followed by PR_3 and base. However, the ability of these intermediates to react with alkynes to generate pyrroles is dependent upon the nature of the PR_3 group. For example, the reaction of *p*-Tol(H)C═NBn (*p*-Tol = *p*-$CH_3C_6H_4$, Bn = CH_2Ph) and *p*-methoxybenzoyl chloride, followed by PPh_3, results in the near-quantitative formation of the phosphonium salt **5** within minutes at ambient temperature. However, the addition of LiHMDS followed by dimethyl acetylenedicarboxylate does not result in pyrrole formation, even at elevated temperatures (Table 1, entry 1). In contrast, the same series of steps with PPh(*o*-$O_2C_6H_4$) (PPh(catechyl)) provides a high yield of pyrrole within 5 min at ambient temperature (entry 2).

A range of other phosphorus reagents were examined. Relatively electron-rich alkyl-substituted phosphines can be incorporated into **2**/**3** (entries 3 and 4), but they are unable to mediate cycloaddition with DMAD. Electron-poor phosphites are also unable to mediate pyrrole formation (entries 6 and 7), but this is because poor nucleophilicity (triphenylphosphite) or competing Arbuzov product formation (triethyl phosphite)[14,15]

(9) For recent alternative Münchnone syntheses, see: (a) Merlic, C. A.; Baur, A.; Aldrich, C. C. *J. Am. Chem. Soc.* **2000**, *122*, 7398. (b) Alper, H.; Tanaka, M. *J. Am. Chem. Soc.* **1979**, *101*, 4245. (c) Keating, T. A.; Armstrong, R. W. *J. Am. Chem. Soc.* **1996**, *118*, 2574.

(10) For representative examples, see: (a) Funabiki, K.; Ishihara, T.; Yamanaka, H.. *J. Fluorine Chem.* **1995**, *71*, 5. (b) Anderson, W. K.; Corey., P. F. *J. Org. Chem.* **1977**, *42*, 559. (c) Texier, F.; Mazari, M.; Yebdri, O.; Tonnard, F.; Carrié, R. *Bull. Soc. Chim. Fr.* **1991**, *128*, 962.

(11) (a) Dhawan, R.; Arndtsen, B. A. *J. Am. Chem. Soc.* **2004**, *126*, 468. (b) Dhawan, R.; Dghaym, R.; Arndtsen, B. A. *J. Am. Chem. Soc.* **2003**, *125*, 1474. (c) For an alternative isocyanide-mediated approach, see: St. Cyr, D. J.; Martin, N.; Arndtsen, B. A. *Org. Lett.* **2007**, *9*, 449.

(12) St. Cyr, D. J.; Arndtsen, B. A. *J. Am. Chem. Soc.* **2007**, *129*, 12366.

(13) Krenske, E. H.; Houk, K. N.; Arndtsen, B. A.; St. Cyr, D. J. *J. Am. Chem. Soc.* **2008**, *130*, 10052.

(14) (a) Colle, K. S.; Lewis, E. S. *J. Org. Chem.* **1978**, *43*, 571. (b) Arbuzov reaction review: Bhattacharya, A. K.; Thyagarajan, G. *Chem. Rev.* **1981**, *81*, 415.

(15) For routes to alkoxy-substituted Wittig reagents, see: (a) Aggarwal, V. K.; Fulton, J. R.; Sheldon, C. G.; de Vicente, J. *J. Am. Chem. Soc.* **2003**, *125*, 6034. (b) Kolodiazhnyi, O. I. *Phosphorus Ylides: Chemistry and Application in Organic Synthesis*; Wiley-VCH: Weinheim, 1999. (c) Johnson, A. W. *Ylides and Imines of Phosphorus*; Wiley-Interscience: New York, 1993.

TABLE 1. Effect of PR_3 on Pyrrole Synthesis[a]

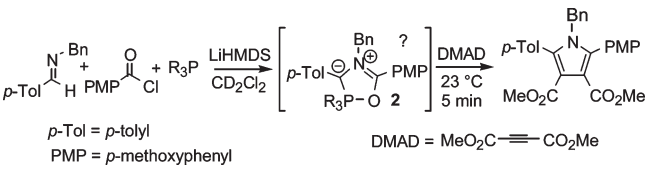

no.	PR_3	^{31}P of **2** (ppm)	additive	yield[b] (%)
1	PPh_3	10.2		0
2	PhP(catechyl)	−16.9		85
3	PCy_3	22.5		0
4	PMe_3	−1.9		0
5	$P(NMe_2)_3$	51.3		0
6	$P(OEt)_3$	[c]		
7	$P(OPh)_3$			
8	$P(OEt)_3$	44.4	TMSOTf	0
9	$P(OPh)_3$	30.2, −44.0 (1.2:1)	TMSOTf	94
10	$P(OCH_2CF_3)_3$	47.0, −21.3 (1.8:1)	TMSOTf	92
11	PF(catechyl)	−22.0[d]	TMSOTf	61
12	PPh_2Cl	[e]	TMSOTf	

[a]Imine (41.9 mg, 0.200 mmol), acid chloride (34.1 mg, 0.200 mmol), 0.7 mL of CD_2Cl_2, rt, 1 h; followed by additive (0.200 mmol), PR_3 (0.200 mmol), rt; LiHMDS solution (0.22 mL, 0.220 mmol), −78 °C to rt; DMAD (74 μL, 0.60 mmol), rt, 5 min. [b]Isolated. [c]Arbuzov product obtained. [d]$^1J_{PF}$ = 1296.2 Hz. [e]**5** was formed, but deprotonation failed to yield **2**.

SCHEME 2. Mechanism of Formation of 2

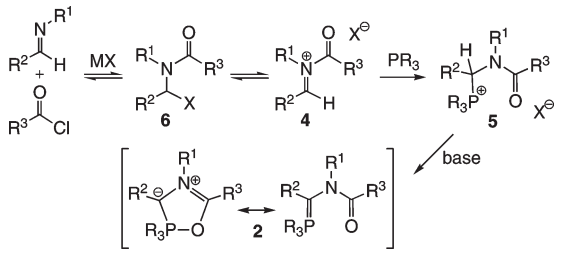

hampers the formation of phosphonium salt **5** (Scheme 2). This problem is eliminated by the addition of TMSOTf, which shifts the **4/6** equilibrium (Scheme 2, X = Cl) toward the reactive *N*-acyliminium form **4** (X = OTf). Use of TMSOTf allowed formation of pyrroles from commercially available triphenyl phosphite and tris(trifluoroethyl) phosphite (entries 9 and 10)[16] and even from the very weakly nucleophilic PF-(catechyl) (although in low yield; entry 11). The slightly more electron-rich counterparts, $P(OEt)_3$ (entry 8) and $P(NMe_2)_3$ (entry 5), however, did not mediate cycloaddition.

While several PR_3 groups lead to high yields of pyrrole from DMAD, the yields are more variable for other alkynes. For example, methyl propiolate reacts with each of the substrates that were found to be reactive in Table 1 but only gives a high yield of pyrrole with PPh(catechyl) (Table 2, entry 3). Similar results are observed with 1,1-chlorocyanoethylene (entries 4−6).

We postulated that the PR_3 reagent must strike a balance between having sufficient nucleophilicity to attack the *N*-acyliminium salt **4** and being sufficiently electron poor to accept chelation of the amide oxygen and generate the 1,3-dipole **2**. The ^{31}P NMR chemical shifts of the intermediates

(16) Compound **2** can also be prepared from $P(OPh)_3$ and $P(OCH_2CF_3)_3$ by waiting several hours before base addition, instead of via TMSOTf addition (Yield **2**: $P(OCH_2CF_3)_3$ = 90%, $P(OPh_3)$ = 98%, PhP(catechyl) = 91%). $ClCH_2CF_3$ formation from **5** (R = OCH_2CF_3, X = Cl, Scheme 2) is slow at rt.

TABLE 2. Effect of PR_3 Reagent and Dipolarophile on Cycloaddition Yields[a]

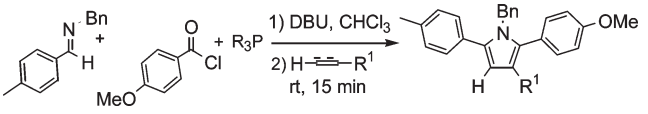

no.	PR_3	alkyne or alkene	R^1	yield[b] (%)
1[c]	$P(OPh)_3$	≡—CO_2Me	CO_2Me	54
2[c]	$P(OCH_2CF_3)_3$	≡—CO_2Me	CO_2Me	50
3	PPh(catechyl)	≡—CO_2Me	CO_2Me	88
4[c]	$P(OPh)_3$	Cl, CN	CN	58
5[c, d]	$P(OCH_2CF_3)_3$	Cl, CN	CN	57
6	PPh(catechyl)	Cl, CN	CN	90

[a]Imine (41.9 mg, 0.200 mmol), acid chloride (34.1 mg, 0.200 mmol), 0.7 mL of $CHCl_3$, 30 min; followed by PR_3 (0.300 mmol), DBU (60 μL, 0.4 mmol); alkyne (0.600 mmol), 15 min. [b]Isolated. [c]Imine/acid chloride/PR_3 for 72 h [$P(OPh_3)$] or 0.5 h [$P(OCH_2CF_3)_3$] prior to DBU.[16] [d]6 equiv of alkene.

2/3, shown in Table 1, correlate with the 1,3-dipolar reactivities. In general, intermediates that are unreactive toward alkynes (entries 1 and 3−8) have ^{31}P NMR resonances in the typical region for related Wittig-type reagents,[17] while intermediates that undergo 1,3-dipolar cycloaddition have upfield resonances (δ −16.9 to −44.0; entries 2 and 9−11). Interestingly, two different signals are observed with the phosphites $P(OPh)_3$ and $P(OCH_2CF_3)_3$, implying that two structures are present in solution.[18] These data suggest that the electronic and steric features of the PR_3 unit can significantly influence the ground state structure and both the cyclic species **2** and the acyclic species **3** may exist in solution.

II. NMR and X-ray Crystallographic Characterization of 2b and 3a. We have isolated and examined the structure of an example of each type of intermediate: an acyclic intermediate, **3a**, generated with PPh_3, and a cyclic intermediate, **2b**, generated with PhP(catechyl).

NMR and X-ray Characterization of PPh_3-Based 3a. The triphenylphosphine-based **3a** (R^1 = Me, R^2 = R^3 = Ph) can be isolated in 82% yield after BuLi deprotonation of in situ generated **5a** (Scheme 2). The carbonyl unit derived from the acid chloride has a ^{13}C NMR signal at 176.1 ppm. This is in a similar region to that expected for a simple amide and shows none of the perturbation expected for an interaction of the amide oxygen with the organophosphorus unit. The ^{31}P NMR signal of **3a**, at 11.0 ppm, matches that observed when

(17) Phosphorus ylides typically show ^{31}P NMR = δ +40 to −9 ppm, while five-coordinate phosphorus appears at δ +10 to −90 ppm . *Handbook of Phosphorus-31 NMR Data*; Tebby, J. C., Ed.; CRC Press: Boston, 1991; and ref 15c.

(18) The ratios of these two ^{31}P NMR signals are temperature dependent, consistent with their presence in dynamic equilibrium.

generated in situ (Table 1), falling in the typical region for PPh_3-based Wittig reagents.[17]

The acyclic structure of **3a** was confirmed by X-ray crystallography.[19,20] Slow diffusion of diethyl ether into a benzene solution of **3a** provided crystals suitable for X-ray analysis. The resulting ORTEP is shown in Figure 2. Compound **3a** adopts an acyclic, Wittig-like structure in the ground state, with no interaction between phosphorus and the amide oxygen. The amide carbonyl oxygen O(3) is oriented away from phosphorus, at a distance of 4.443 Å. The carbonyl and C(13)−N(1) bond lengths and angles are typical of simple amides [C(13)−O(3), 1.229 Å; N(1)−C(13), 1.366 Å].[21] A torsion of 78.3° around C(13)−N(1)−C(14)−P places the nitrogen lone pair nearly perpendicular to the P−C(14) π-system, minimizing the destabilizing interaction with the carbanion lone pair at C(14). The P−C(14) bond length of 1.719 Å and the pseudotetrahedral configuration at phosphorus are both similar to those in related phosphorus ylides.[15,22]

NMR and X-ray Structural Characterization of PPh-(catechyl)-Based 2b. The PPh(catechyl)-based **2b** (R^1 = Me, $R^2 = R^3$ = Ph) was isolated by precipitation from acetonitrile and has ^{13}C and ^{31}P NMR data quite distinct from those of **3a**. The ^{13}C NMR resonance of the carbonyl unit shows a strong upfield shift, to 149.2 ppm, suggesting disruption of the amide substructure. The ^{31}P NMR resonance, at −18.9 ppm, is upfield of classic Wittig-type reagents, falling instead in the diagnostic range for five-coordinate organophosphorus compounds.[17]

The crystal structure (Figure 3) confirms that **2b** represents a new class of 1,3-dipole in the ground state. The phosphorus center adopts a five-coordinate, pseudotrigonal bipyramidal geometry, with the axial sites occupied by one catechyl oxygen [O(1)] and the O(3) oxygen from the former amide unit. There is a strong interaction between the former amide oxygen and phosphorus (P−O(3) = 1.789 Å).[23,24] This bond is longer than typical $P-O_{axial}$ bonds (1.689 Å) but

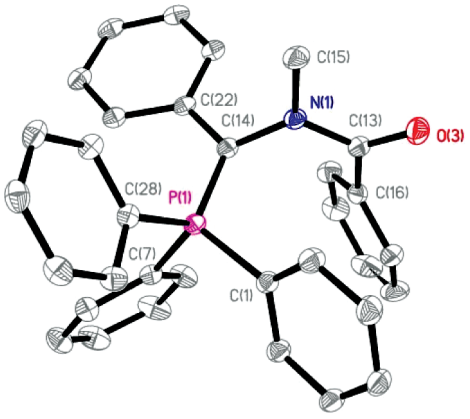

FIGURE 2. X-ray crystal structure of **3a** (ORTEP view). Hydrogens have been removed for clarity, and displacement ellipsoids are scaled to the 30% probability level. Selected bond lengths (Å) and angles (deg): P(1)−C(14), 1.7189(14); P(1)−C(1), 1.8101(14); P(1)−C(7), 1.8107(14); P(1)−C(28), 1.8296(14); N(1)−C(13), 1.3660(18); N(1)−C(14), 1.4356(18); N(1)−C(15), 1.4652(18); O(3)−C(13), 1.2286(18); C(14)−C(22), 1.4529(19); C(13)−C(16), 1.501(2); C(14)−P(1)−C(1), 112.55(7); C(14)−P(1)−C(7), 109.36(7); C(14)−P(1)−C(28), 118.36(7); C(1)−P(1)−C(7), 106.98(7); C(1)−P(1)−C(28), 101.94(6); C(7)−P(1)−C(28), 106.87(6); C(13)−N(1)−C(14), 123.89(12); C(13)−N(1)−C(15), 117.45(12); C(14)−N(1)−C(15), 118.35(11); O(3)−C(13)−N(1), 121.87(13); O(3)−C(13)−C(16), 120.21(13); N(1)−C(13)−C(16), 117.89(12); N(1)−C(14)−C(22), 118.25(12); N(1)−C(14)−P(1), 118.12(10); C(22)−C(14)−P(1), 122.09(10).

shorter than those typically observed in cyclic $R_nP\cdots O$ Lewis acid/base adducts.[25] The carbonyl C(13)−O(3) bond shows diminished double-bond character (1.317 Å,[26] compared with 1.229 Å in **3a**), and the N(1)−C(13) bond shows increased double-bond character (1.316 Å, compared with 1.366 Å in **3a**),[27] consistent with a strong iminium contribution to the former amide moiety.

The P(1)−C(14) bond length in **2b** is similar to that in classical Wittig reagents (1.706 Å)[15c] and is even slightly shorter than that in **3a** (1.719 Å). The C(1)−P(1)−O(2) equatorial bond angle is compressed from the ideal 120° to 105.7°. These features are consistent with P(1)=C(14) multiple bonding, which is expected to perturb the P(1)−O(2) and P(1)−C(1) σ-bonds in the trigonal plane due to hyperconjugation with the C(14) carbanion.[28]

Structural Comparison of 2b to Münchnones. Structural data for **2b** and the analogously substituted Münchnone **1a**[29a] are shown in Figure 4.

The Münchnone ring in **1a** is virtually planar, whereas in **2b**, the oxygen is 0.050 Å out of the plane formed by the remaining ring atoms. The substitution of PR_3 for the carbonyl unit yields a wider C−N−C angle (113.8° vs 109.6°), increasing the steric crowding about the ring in **2b**. Outside of these differences, however, the pattern of bond

(19) Solid-state ^{31}P NMR confirms consistency between the solution-phase and solid-state structures; see the Experimental Section.

(20) For examples of related amino-substituted phosphorus ylides, see: (a) Paterson, I.; Cowden, C.; Watson, C. *Synlett* **1996**, *3*, 209. (b) Canac, Y.; Conejero, S.; Soleilhavoup, M.; Donnadieu, B.; Bertrand, G. *J. Am. Chem. Soc.* **2006**, *128*, 459.

(21) Allen, F. H.; Kennard, O.; Watson, D. G.; Brammer, L.; Orpen, A. G.; Taylor, R. *J. Chem. Soc., Perkin Trans. 2* **1987**, *12*, S1–S19.

(22) For the crystal structure of $Ph_3P{=}C(H)Ph$, see: Yufit, D. S.; Howard, J. A. K.; Davidson, M. G. *J. Chem. Soc., Perkin Trans. 2* **2000**, *2*, 249.

(23) For related phosphorus complexes, see: (a) Burger, K.; Fuchs, A. *Nitrogen, Oxygen and Sulfur Ylide Chemistry*; Clark, S. J., Ed.; Oxford University Press: Oxford, UK, 2002; Chapter 4, pp 286−292. (b) Onys'ko, P. P.; Rassukana, Y. V.; Sinitsa, A. D. *Curr. Org. Chem.* **2008**, *12*, 2. (c) Stieglitz, G.; Neumueller, B.; Dehnicke, K. Z.; Naturforsch., B *Chem. Sci.* **1993**, *48*, 730. (d) Matsukawa, S.; Kojima, S.; Kajiyama, K.; Yamamoto, Y.; Akiba, K.-Y.; Re, S.; Nagase, S. *J. Am. Chem. Soc.* **2002**, *124*, 13154. (e) Satoshi Kojima, S.; Takagi, R.; Akiba, K. *J. Am. Chem. Soc.* **1997**, *119*, 5970. (f) Naya, S.-i.; Nitta, M. *J. Chem. Soc., Perkin Trans. 2* **2002**, *5*, 1017. (g) Kano, N.; Kikuchi, A.; Kawashima, T. *Chem. Commun.* **2001**, 2096.

(24) Examples of $R_3P{=}X$ (X = O, S, NR) with intramolecular coordination: (a) Chuit, C.; Reyé, C. *Eur. J. Inorg. Chem.* **1998**, *1*, 1847. (b) Holmes, R. R. *Acc. Chem. Res.* **1998**, *31*, 535. (c) Kumaraswamy, S.; Muthiah, S. K. C. K. *J. Am. Chem. Soc.* **2000**, *122*, 964. (d) Schomburg, D.; Wermuth, U.; Schmutzler, R. *Phosphorus, Sulfur Silicon Relat. Elem.* **1986**, *26*, 193.

(25) For examples, see: (a) Cavell, R. G; Vande Griend, L. *Inorg. Chem.* **1986**, *25*, 4699. (b) Cavell, R. G.; The, K. I.; Van de Griend, L. *Inorg. Chem.* **1981**, *20*, 3813. (c) Lacour, J.; Vial, L.; Bernardinelli, G. *Org. Lett.* **2002**, *4*, 2309. (d) Burford, N.; Kennepohl, D.; Cowie, M.; Ball, R. G.; Cavell, R. G. *Inorg. Chem.* **1987**, *26*, 650–657. (e) Chandrasekaran, A.; Day, R. O.; Holmes, R. R. *Inorg. Chem.* **2001**, *40*, 6229.

(26) The C−O single bond is > 1.30 Å.[21]

(27) The 1.316 Å C−N bond length is shorter than the average for amides (1.34 Å, see ref 21) and longer than the < 1.30 Å of related iminium structures: (a) Li, P.; Xu, J. C. *J. Chem. Soc., Perkin Trans. 2* **2001**, *1*, 113. (b) Krill, J.; Shevchenko, I. V.; Fischer, A.; Jones, P. G.; Schmutzler, R. *Chem. Ber. Recl.* **1997**, *130*, 1479.

(28) Leyssens, T.; Peeters, D. *J. Org. Chem.* **2008**, *73*, 2725.

(29) (a) Toupet, L.; Texier, F.; Carrie, R. *Acta Crystallogr., Sect. C: Cryst. Struct. Commun.* **1991**, *C47*, 328. (b) Boyd, G. V.; Davies, C. G.; Donaldson, J. D.; J. Silver, J.; Wright, P. H. *J. Chem. Soc., Perkin Trans. 2* **1975**, *12*, 1280.

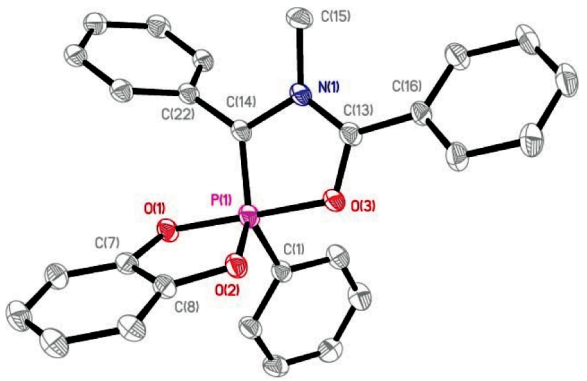

FIGURE 3. X-ray crystal structure of **2b**·C_6H_6 (ORTEP view). Hydrogens and solvent have been removed for clarity, and displacement ellipsoids are scaled to the 30% probability level. Selected bond lengths (Å) and angles (deg): P(1)−O(2), 1.6772(19); P(1)−C(14), 1.706(3); P(1)−O(1), 1.7281(18); P(1)−O(3), 1.7894(18); P(1)−C(1), 1.824(3); O(3)−C(13), 1.317(3); N(1)−C(13), 1.316(3); N(1)−C(14), 1.434(3); N(1)−C(15), 1.475(4); C(13)−C(16), 1.462(4); C(14)−C(22), 1.473(4); O(2)−P(1)−C(14), 126.90(12); O(2)−P(1)−O(1), 90.71(9); C(14)−P(1)−O(1), 93.09(11); O(2)−P(1)−O(3), 85.77(9); C(14)−P(1)−O(3), 86.78(11); O(1)−P(1)−O(3), 175.48(9); O(2)−P(1)−C(1), 105.66(12); C(14)−P(1)−C(1), 126.96(13); O(1)−P(1)−C(1), 92.85(11); O(3)−P(1)−C(1), 90.83(11); C(13)−O(3)−P(1), 114.86(17); C(13)−N(1)−C(14), 113.8(3); C(13)−N(1)−C(15), 124.5(2); C(14)−N(1)−C(15), 120.5(2); N(1)−C(13)−O(3), 112.5(2); N(1)−C(13)−C(16), 128.2(3); O(3)−C(13)−C(16), 119.2(3); N(1)−C(14)−C(22), 118.3(3); N(1)−C(14)−P(1), 111.9(2); C(22)−C(14)−P(1), 129.6(2).

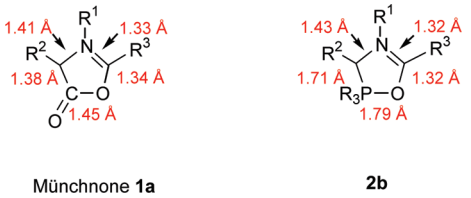

Münchnone **1a** **2b**

FIGURE 4. Structural comparison of Münchnone **1a** (R^1 = Me, R^2 = Ph, R^3 = *p*-methoxyphenyl)[29a] and **2b** (R^1 = Me, R^2 = R^3 = Ph), with approximate ring bond lengths.

lengths in **2b** is remarkably similar to that in **1a**. Both structures show lengthened C(R^3)−O bonds (1.317 and 1.337 Å) and shortened C(R^3)−N bonds (1.316 and 1.332 Å), consistent with significant C(R^3)−N iminium character. The C(14)−N(1) bonds (1.434 and 1.411 Å) are close to single-bond length,[24] while the P−C(R^2) and C(=O)−C(R^2) bonds are intermediate between single and double bond values, at 1.706 and 1.375 Å, respectively.[15c,24] In considering the various viable resonance structures for **2b**, these data favor dipolar structures A and B (Figure 5), analogous to Münchnones. Compound **2b** mirrors not only the reactivity, but also the ground-state structure, of Münchnones.[5]

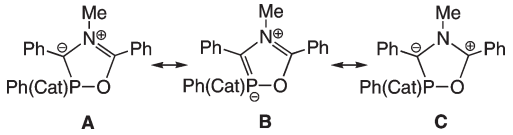

FIGURE 5. Limiting resonance structures of **2b**.

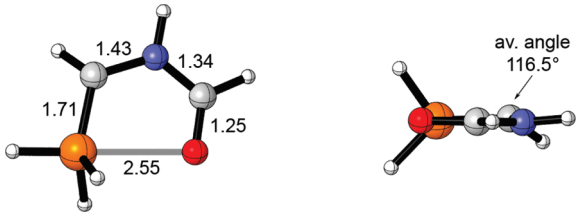

FIGURE 6. Geometry of **2d** (bond lengths in Å).

III. Computational Studies of Geometries. To explore the sensitivity of dipole structure and stability to substituent effects, we performed density functional theory calculations at the B3LYP/6-31+G(d) level in Gaussian 03.[30] In previous studies on the parent dipole **2d**,[13] a range of ab initio and density functional methods gave very similar geometries (P−O distances ranging from 2.51 to 2.57 Å) and differences in energy $\Delta H_{cyc-acyc}$ between the cyclic form **2d** and acyclic form **3d** ($\Delta H_{cyc-acyc}$ in the range −1.7 to −3.1 kcal mol^{-1}). Two views of **2d** at the B3LYP/6-31+G(d) level are shown in Figure 6. The long P−O distance of 2.55 Å and substantial pyramidalization at the ylidic carbon C_P (average bond angle 116.5°) indicate that it is best regarded as an acylaminophosphonium ylide containing an electrostatic P−O interaction and not a covalently bound heterocycle.

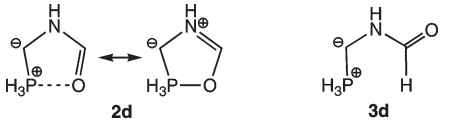

A range of substituted derivatives of **2d** are shown in Figure 7, together with the corresponding energy differences between their cyclic and acyclic forms. A methyl group at nitrogen (**2e**) shortens the P−O bond by 0.11 Å and stabilizes the cyclic form by 3.4 kcal mol^{-1}. A phenyl group at the ylidic carbon (**2f**) shortens the P−O bond by 0.09 Å, while a phenyl group at the carbonyl carbon (**2g**) shortens the P−O bond by 0.18 Å. Together (**2h**), these two groups have an additive effect on the P−O distance (shortened by 0.27 Å) and stabilize the cyclic form by 4.7 kcal mol^{-1} over the acyclic form. The most substantial geometrical effects are exerted, however, by the substituents at phosphorus. Figure 7 shows derivatives containing PPh_3, PMe_3, $P(OMe)_3$, $P(OCH_2)_3CH$, and PPh(catechyl) groups. The P−O distances in the cyclic isomers range from an essentially nonbonded arrangement for PPh_3 (**2i**) (3.92 Å) to a substantially covalent bond for PPh(catechyl) (**2m**) in the O-axial conformation (1.97 Å). The PMe_3, $P(OMe)_3$, and $P(OCH_2)_3CH$ derivatives have P−O distances of 3.05, 2.86, and 2.00 Å, respectively.

(30) *Gaussian 03, Revision C.02*: Frisch, M. J.; Trucks, G. W.; Schlegel, H. B.; Scuseria, G. E.; Robb, M. A.; Cheeseman, J. R.; Montgomery, J. A., Jr.; Vreven, T.; Kudin, K. N.; Burant, J. C.; Millam, J. M.; Iyengar, S. S.; Tomasi, J.; Barone, V.; Mennucci, B.; Cossi, M.; Scalmani, G.; Rega, N.; Petersson, G. A.; Nakatsuji, H.; Hada, M.; Ehara, M.; Toyota, K.; Fukuda, R.; Hasegawa, J.; Ishida, M.; Nakajima, T.; Honda, Y.; Kitao, O.; Nakai, H.; Klene, M.; Li, X.; Knox, J. E.; Hratchian, H. P.; Cross, J. B.; Bakken, V.; Adamo, C.; Jaramillo, J.; Gomperts, R.; Stratmann, R. E.; Yazyev, O.; Austin, A. J.; Cammi, R.; Pomelli, C.; Ochterski, J. W.; Ayala, P. Y.; Morokuma, K.; Voth, G. A.; Salvador, P.; Dannenberg, J. J.; Zakrzewski, V. G.; Dapprich, S.; Daniels, A. D.; Strain, M. C.; Farkas, O.; Malick, D. K.; Rabuck, A. D.; Raghavachari, K.; Foresman, J. B.; Ortiz, J. V.; Cui, Q.; Baboul, A. G.; Clifford, S.; Cioslowski, J.; Stefanov, B. B.; Liu, G.; Liashenko, A.; Piskorz, P.; Komaromi, I.; Martin, R. L.; Fox, D. J.; Keith, T.; Al-Laham, M. A.; Peng, C. Y.; Nanayakkara, A.; Challacombe, M.; Gill, P. M. W.; Johnson, B.; Chen, W.; Wong, M. W.; Gonzalez, C.; Pople, J. A. Gaussian, Inc., Wallingford CT, 2004.

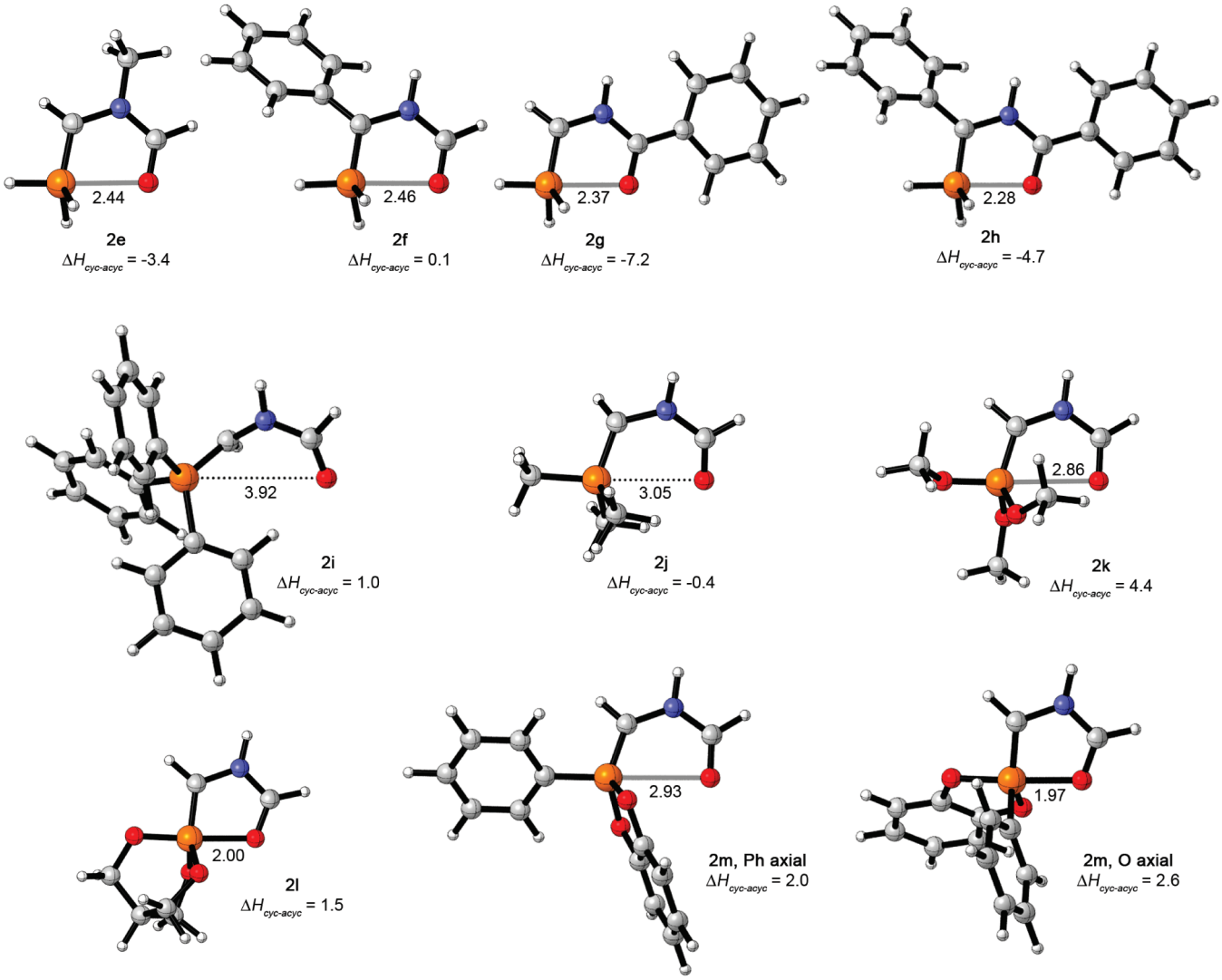

FIGURE 7. Geometries and cyclic−acyclic energy differences of various derivatives of **2** (bond lengths in Å; $\Delta H_{cyc-acyc}$ in kcal mol^{-1}).

CHART 1

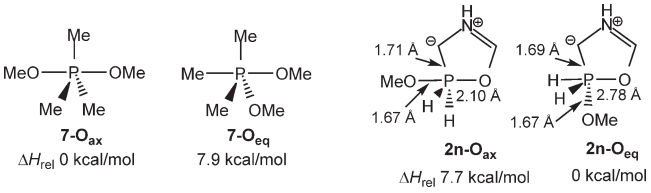

Taking into account the effects of the C- and N-substituents on the P−O bond, the calculated structures are in close agreement with the X-ray crystal structures of the PPh_3 and PPh(catechyl) derivatives **3a** and **2b**.

The apicophilicity of an alkoxy group at phosphorus in the dipoles **2** differs from that in typical 5-coordinate phosphorus derivatives. For example, whereas the phosphorane **7** (Chart 1) is 7.9 kcal mol^{-1} more stable with both OMe groups axial than with one axial and one equatorial, the ylide **2n** is 7.7 kcal mol^{-1} more stable with OMe equatorial. In **2n-O$_{eq}$**, negative hyperconjugation between the carbanion lone pair and the antiperiplanar P−OMe σ^* orbital results in net stabilization, even though simultaneous negative hyperconjugation between an OMe lone pair and the intracyclic P−O antibonding orbital weakens the intracyclic P−O interaction by 0.68 Å. These features also operate in the PPh(catechyl) derivative **2m**. The Ph-axial conformer of **2m** is 0.6 kcal mol^{-1} more stable than the O-axial form, but its P−O distance is almost 1 Å longer. The smaller energy difference between the two conformers of **2m** compared with **2n** reflects the geometrical preference of the catechyl group to occupy an equatorial/axial arrangement rather than bridging two pseudoequatorial positions.

IV. Structural Effects on Cycloaddition Barriers. Insights into the widely diverging 1,3-dipolar cycloaddition efficiencies for different PR_3 groups are provided by the transition states for cycloadditions with ethylene. Three representative transition-state (TS) geometries are shown in Figure 8. In the TS for the parent dipole **2d**, the bond developing at the carbonyl carbon is 0.2 Å shorter than that at the ylidic carbon. A similarly polarized but more asynchronous TS is found for the PPh(catechyl) derivative **2m**. In contrast, the PPh_3-containing dipole **2i** shows more advanced bond development at the ylidic carbon, consistent with the Wittig reagent-like structure of the reactant dipole.

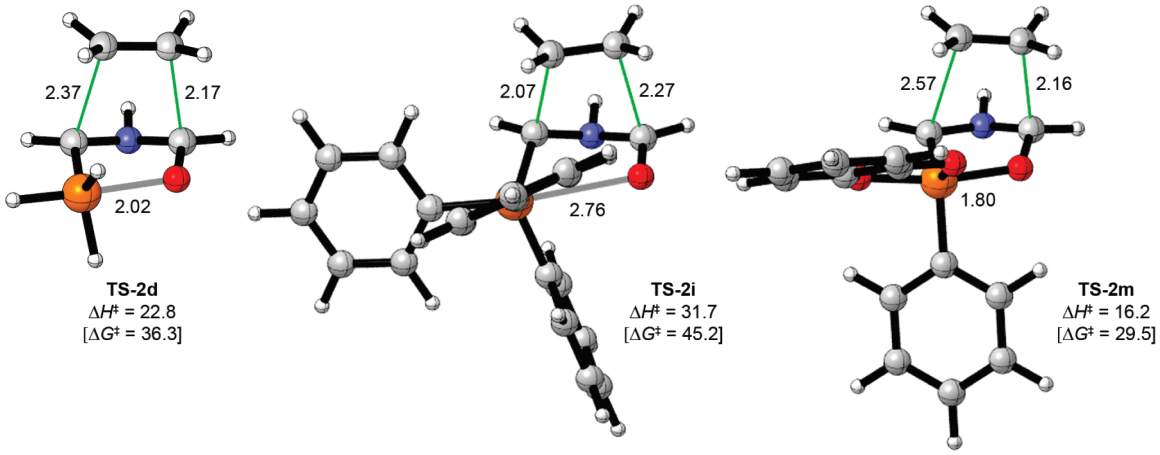

FIGURE 8. Transition structures for concerted cycloaddition of **2d**, **2i**, and **2m** (O-axial) with ethylene (bond distances in Å; barriers in kcal mol^{-1}).

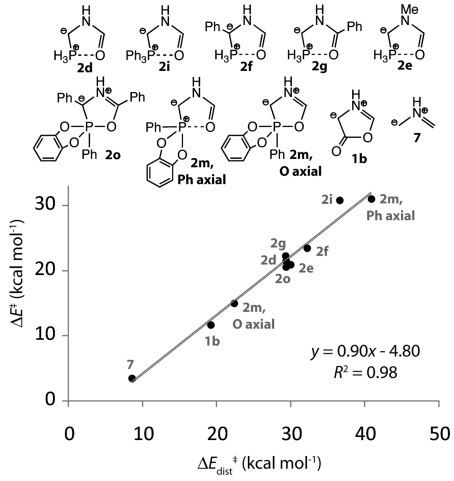

FIGURE 9. Plot of activation energies vs distortion energies for concerted cycloadditions of 1,3-dipoles with ethylene.

Consistent with experiment, the PPh_3-containing dipole has a high activation energy of $\Delta H^{\ddagger} = 31.7$ kcal mol^{-1}, while the activation energy for the PPh(catechyl) derivative is 16.2 kcal mol^{-1}. The activation energies for the three TSs in Figure 8 follow the same trend as the degree to which the P−O bond must shorten to reach the TS; for PPh_3, the dipole must decrease its P−O separation by 1.16 Å, whereas for PPh(catechyl) a shortening of only 0.17 Å is required. More generally, the activation energies ($\Delta E^{\ddagger}$) for cycloadditions of 1,3-dipoles such as **2** with ethylene correlate with the energy ($\Delta E_{dist}^{\ddagger}$) required to distort the reactants from their ground-state geometries to their TS geometries. In Figure 9 is shown a plot of $\Delta E^{\ddagger}$ versus $\Delta E_{dist}^{\ddagger}$ for eight representative ylidic dipoles, along with those for the parent Münchnone and azomethine ylide. There is a very close correlation ($R^2 = 0.98$) between $\Delta E^{\ddagger}$ and $\Delta E_{dist}^{\ddagger}$. Similar correlations have previously been noted for 1,3-dipolar cycloadditions of azomethine, nitrilium, and diazonium betaines with ethylene and acetylene,[31] as well as for cycloadditions of azides with alkenes and alkynes.[32] For those acyclic 1,3-dipoles, bending about the central atom contributes the major fraction of the dipole distortion energy,[33] whereas for the ylidic dipoles in Figure 9 the major geometrical change required to reach the TS is P−O compression; there is a correlation of $R^2 = 0.57$ between dipole distortion energy and the change in P−O distance on going from reactant to TS.

V. Cycloadditions with Substituted Alkynes. Although concerted transition states are found for the reactions of **2** with ethylene, it is possible that cycloadditions with electron-deficient alkynes follow stepwise mechanisms. In Figure 10 are shown the two regioisomeric transition states for the reaction of **2o** with cyanoacetylene. The favored cycloaddition mechanism is a stepwise pathway in which **2o** adds nucleophilically to the terminal carbon of cyanoacetylene, forming a CN-stabilized carbanion that then closes onto the iminium group to provide the bicyclic product. Formation of the opposite regioisomer could occur by a concerted mechanism but is disfavored by 6.8 kcal mol^{-1} ($\Delta\Delta H^{\ddagger}$). High regioselectivity is exerted through electronic control.

We also investigated the possibility that the carbanion in the zwitterionic intermediate may add to phosphorus instead of to the carbonyl group. Subsequent scission of the original P−C bond could lead to a CN-stabilized ylide that then undergoes an intramolecular Wittig reaction with the amide carbonyl. However, in the parent species **2d**, the activation energy for ring closure onto phosphorus is 4.7 kcal mol^{-1} higher than for closure onto carbonyl, and for the more highly substituted **2o**, steric crowding at phosphorus renders such a pathway unfeasible.

VI. Cycloaddition Regioselectivities. There is a much greater electronic bias across the dipole in **2** than in Münchnones. For example, the charges at the ylidic carbon and carbonyl carbon in **2d**, calculated by the natural bond orbital method,[34] are −0.78 and +0.46, respectively, compared to −0.33 and +0.38 for the parent Münchnone. This feature suggests that regioselective cycloadditions may be possible.

(31) (a) Ess, D. H.; Houk, K. N. *J. Am. Chem. Soc.* **2007**, *129*, 10646–10647. (b) Ess, D. H.; Houk, K. N. *J. Am. Chem. Soc.* **2008**, *130*, 10187–10198.

(32) (a) Ess, D. H.; Jones, G. O.; Houk, K. N. *Org. Lett.* **2008**, *10*, 1633–1636. (b) Schoenebeck, F.; Ess, D. H.; Jones, G. O.; Houk, K. N. *J. Am. Chem. Soc.* **2009**, *131*, 8121–8133.

(33) Xu, L.; Doubleday, C. E.; Houk, K. N. *Angew. Chem., Int. Ed.* **2009**, *48*, 2746–2748.

(34) Glendening, E. D.; Reed, A. E.; Carpenter, J. E.; Weinhold, F. NBO Version 3.1.

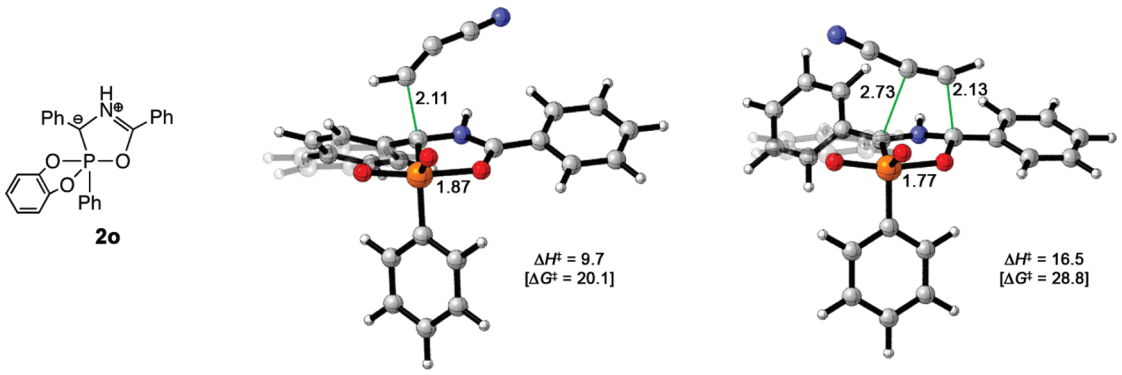

FIGURE 10. Regioisomeric transition structures for cycloaddition of **2o** with cyanoacetylene (bond distances in Å; barriers in kcal mol^{-1}).

TABLE 3. Cycloaddition Regioselectivity with 2[a]

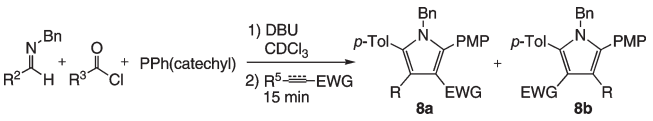

no.	R^2	R^3	alkyne or alkene	yield	**8a**: **8b**
1	*p*-Tol	PMP	≡—CO_2Me	88	> 95: 5
2	*p*-Tol	PMP	Cl, CN	92	> 95: 5
3[b]	*p*-Tol	PMP	Me—≡—CO_2Me	52	> 95: 5
4	PMP	*p*-Tol	Cl, CN	92	< 5: 95
5	PMP	*p*-Tol	≡—CO_2Me	91	< 5: 95
6[b]	PMP	*p*-Tol	Me—≡—CO_2Me	47	< 5: 95

[a]Table 2 procedure.[36] [b]19 h.

The calculated activation energies for cyanoacetylene (section V) indicate that high stereoselectivity can be expected for suitably substituted dipolarophiles.

We have explored this possibility by using dipoles in which the aromatic units on the imine carbon (R^2) and acid chloride (R^3) vary only in the *para*-substituents. As shown in Table 3, the reaction of **2** with methyl propiolate results in a single regioisomer of the pyrrole, where the alkyne ester functional group has been directed toward the former acid chloride substituent (entry 1).[35,36] Similar results are observed with 1-chloro-1-cyanoethylene (entry 2) and the internal alkyne in entry 3, both of which provide the product expected from the electronic bias in **2**. Notably, the electronic bias in **2** is independent of the substituents, including those on the phosphorus unit (Table 2). This contrasts with the reactivity of Münchnones,[5,10] and indeed many other 1,3-dipoles[1] and Diels–Alder substrates,[37] where the substituents on the 4π component are often the determining feature for cycloaddition selectivity. With **2**, exchanging the acid chloride and imine substituents allows access to regioisomeric pyrroles (Table 3, entries 4–6). Derivatives of **2** bearing either electron-rich or electron-poor aryl or alkyl substituents each undergo cycloaddition with terminal alkynes to form a single regioisomer of the pyrrole (vide infra).

A diverse range of polysubstituted pyrroles can be accessed. Examples are shown in Table 4. Variation of the imine component provides examples including *N*-aryl-, alkyl-, allyl-, and benzyl-substituted pyrroles (entries 1–4 and 14–16) and a range of *C*-aromatic and *C*–heteroaromatic derivatives (entries 4–7, 12, 15, and 16). Less stable imines, such as those with enolizable *C*-alkyl groups and even formaldehyde-derived imines (entries 9 and 10), can also be used to generate 2-alkyl- and 2-H-pyrroles. The former is notable, since the iminium salts generated from enolizable imines are prone to enamide formation and are not viable in our previously reported palladium-catalyzed Münchnone synthesis.[11a] The rapid attack of the phosphonite on the in situ generated iminium salt **4** likely allows their use with **2**. Smaller imine *C*-alkyl groups, e.g., *n*-butyl, were not successful. Isoquinoline can be employed as a less reactive imine equivalent, leading to the direct formation of naphthyl-fused pyrrole (entry 11), though in lower yields. From the acid chloride component, aryl, heteroaryl (entries 4, 12, and 13), and alkyl (entries 6, 8, and 16) units may be incorporated.

Cycloadditions can be performed with a range of alkynes, including DMAD, alkyl propiolates, and unsaturated ketones (entry 12). Compound **2** reacts most efficiently with electron-poor dipolarophiles, although some more electron-rich alkynes (acetylene, propargyl ethers: entries 7 and 13–15) are also viable substrates.[38] In general, the cycloadditions of **2** provide a modular strategy to build up a diversity of substituted pyrroles in one-pot reactions.

Conclusions

Suitably substituted phosphonites or phosphites react with imines and acid chlorides to generate a new class of 1,3-dipolar cycloaddition reagent, the phospha-Münchnones **2**.[39] These

(35) A ca. 2:1 mixture of these pyrroles is generated via Münchnones.[11a]

(36) The regiochemistry of all pyrrole products was determined either by comparison to previously reported compounds or via 1D and 2D NOE NMR experiments. See the Experimental Section and the Supporting Information for spectra and full details.

(37) *The Diels-Alder Reaction: Selected Practical Methods*; Fringuelli, F., Taticchi, A., Eds.; Wiley: Baffins Lane, 2002.

(38) Lower pyrrole yields are due to the instability of the 1,3-dipole over long reaction times with less activated dipolarophiles. The **2** is prone to decompose to form (Cat)PhP=O under these conditions, leading to lower yields.

(39) For the closest related example, a trifluoromethyl-substituted [1,4,2]oxazaphospholine has been shown to behave as a dipole precursor (Burger, K.; Fehn, J.; Moll, E. *Chem. Ber.* **1971**, *104*, 1826). However, a simple phosphorus ylide (e.g., **2**) has not been used as a 1,3-dipole.

TABLE 4. Generality of Regioselective Pyrrole Synthesis[a]

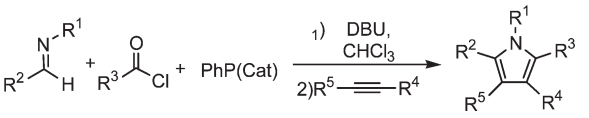

no.	Imine	Acid chloride	Alkyne or Alkene	Pyrrole (%)	no.	Imine	Acid chloride	Alkyne or Alkene	Pyrrole (%)
1		PMPCOCl		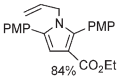 84%	9[c,d]		*p*-TolCOCl		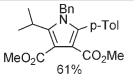 61%
2		PMPCOCl		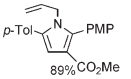 89%	10[e]		PhCOCl		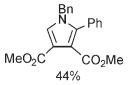 44%
3		*p*-TolCOCl		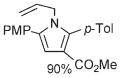 90%	11[f]		PMPCOCl		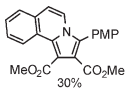 30%
4	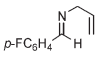			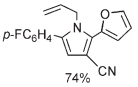 74%	12				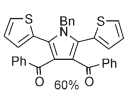 60%
5		*p*-TolCOCl		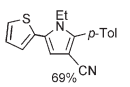 69%	13[g]			H—≡—H	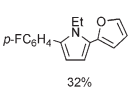 32%
6				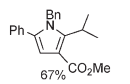 67%	14[g]		PhCOCl	H—≡—H	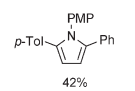 42%
7[b]		*p*-TolCOCl		24%	15[g]		PhCOCl	H—≡—H	35%
8[c]			MeO2C—≡—CO2Me	83%	16[b,c]		^{t}BuCOCl	MeO2C—≡—CO2Me	63%

[a]Table 2 procedure.[36] [b]33 h. [c]LiHMDS at −78 °C, CH_2Cl_2. [d]Imine/acid chloride at −78 °C; AgOTf (1 equiv) added. [e]Imine/acid chloride/PR_3 for 16 h prior to base. [f]TMSOTf (1 equiv) added. [g]1 atm, 50 °C.

dipoles are formally the valence tautomers of amido-substituted Wittig reagents. NMR, X-ray structural, and computational analyses indicate that either form may be preferred, depending upon the PR_3 unit. Electron-poor phosphites and phosphonites more favorably accept oxygen chelation to create the cyclized dipole **2**, while electron-rich phosphines adopt the acyclic Wittig-type structure **3**. The electronegativity of the PR_3 unit is not the only factor, however; $P(OPh)_3$ and $P(OCH_2CF_3)_3$ are less able to stabilize the cyclic form than the more electron-rich PPh(catechyl). Presumably, angle strain involving the catechyl group imparts "strain release Lewis acidity"[40] to the PPh(catechyl) unit, as previously noted for other main group Lewis acids.[41] Angle strain is relieved upon chelation to oxygen, as the catechyl unit then occupies the axial and equatorial sites of the phosphorus trigonal bipyramid. A smaller destabilization of the P−O bond due to negative hyperconjugation might also be expected for the Ph-equatorial PPh(catechyl) group, compared with $P(OPh)_3$. The lower steric bulk of the bidentate catechyl unit likely further strengthens chelation and favors the approach of an alkyne during cycloaddition.

The significant electronic bias introduced by the PR_3 group provides a unique tool to control the cycloaddition regioselectivity. Highly regioselective cycloadditions have been achieved for a diverse range of pyrroles, where the electron-withdrawing group on the dipolarophile is generally directed away from the phosphorus unit during cycloaddition. The regioselective 1,3-dipolar cycloaddition reactivity, together with the easy and modular synthetic protocol, set **2** apart from previously studied 1,3-dipoles such as Münchnones.

(40) Denmark, S. E.; Sweis, R. F. *Acc. Chem. Res.* **2002**, *35*, 835.

(41) (a) Westheimer, F. H. *Acc. Chem. Res.* **1968**, *1*, 70. (b) Kinnaird, J. W. A.; Ng, P. Y.; Kubota, K.; Wang, X.; Leighton, J. L. *J. Am. Chem. Soc.* **2002**, *124*, 7920. (c) Nelson, S. G.; Kim, B.-K.; Peelen, T. J. *J. Am. Chem. Soc.* **2000**, *122*, 9318. (d) Chuit, R. J. P.; Corriu, C.; Reye, J. C.; Young *Chem. Rev.* **1993**, *93*, 1371. (e) Negrebetsky, V. V; Taylor, P. G.; Kramarova, E. P.; Shipov, A. G.; Pogozhikh, S. A.; Ovchinnikov, Y. E.; Korlyukov, A. A.; Bowden, A.; Bassindale, A. R.; Baukov, Y. I. *J. Organomet. Chem.* **2008**, *693*, 1309–1320. (f) Kawashima, T.; Takami, H.; Okazaki, R. *J. Am. Chem. Soc.* **1994**, *116*, 4509.

Experimental Section

General Procedures. All reactions were performed in a drybox or under nitrogen using standard Schlenk techniques. Reagents were used as received, including $PhPCl_2$, catechol, DBU (1,8-diazabicyclo[5.4.0]undec-7-ene), LiHMDS (lithium bis(trimethylsilyl)amide) 1.0 M in hexane or THF, TMSOTf (trimethylsilyl trifluoromethanesulfonate), DMAD (dimethyl acetylenedicarboxylate), aldehydes, amines, and acid chlorides with the following exceptions: Solid PPh_3, PCy_3, and NaF were dried by heating under high vacuum. Liquid $P(OEt)_3$, $P(OCH_2CF_3)$, and $P(NMe_2)_3$ were dried over 4 Å molecular sieves. $P(OPh)_3$ was dried by reflux under high vacuum (ca. 140 °C, ca. 50 mtorr) followed by storage over 4 Å molecular sieves. Dichloromethane and acetonitrile were distilled from CaH_2 under nitrogen. Diethyl ether was distilled from sodium benzophenone ketyl. Chloroform and deuterated chloroform were dried over 4 Å molecular sieves. Imines were prepared as per standard literature procedures.[42] NMR spectra (^1H, ^{13}C, and ^{31}P) were recorded on 200, 300, 400, or 500 MHz spectrometers (for solution-phase spectra) and on a 300 MHz spectrometer (for solid state spectra). Reported J_{C-P} and J_{C-F} values were verified by obtaining ^{13}C NMR spectra at both 300 and 500 MHz. In the X-ray crystallography, nonbonding distance calculations were obtained using the Mercury 1.4.2 CIF visualization software. Pyrroles of Table 3, entries 1 and 5, and Table 4, entries 2, 4−12, and 14, were characterized by comparison to previous literature reports.[11c,12,47]

Computational Methods. Density functional theory calculations were performed at the B3LYP/6-31+G(d) level[43] in Gaussian 03.[30] Species were characterized as minima or transition states on the basis of vibrational frequency analyses and IRC calculations.[44] Conformational searches were carried out in order to identify the lowest energy structure for each species. Zero-point energy and thermal corrections were derived (unscaled) from the B3LYP/6-31+G(d) frequencies. Population analyses were performed with the natural bond orbital method.[34]

Synthesis of PhP(o-$O_2C_6H_4$) [PhP(catechyl)]. A modified version of the literature procedure was followed.[45] To catechol (11.01 g, 100 mmol) under nitrogen in a 500 mL Schlenk flask was added Et_2O (100 mL) followed by pyridine (16.2 mL, 200 mmol). The mixture was cooled to 0 °C, $PhPCl_2$ (13.6 mL, 100 mmol) was added dropwise over 15−45 min with vigorous stirring, and the mixture stirred at ambient temperature for 2 h. The flask was fitted to an air-free filtration assembly for the removal of the pyridine hydrochloride precipitate. The filtrate was concentrated in vacuo without exposure to air and distilled (84−88 °C, 115 mTorr) to afford 12.9 g (60%) of a clear colorless oil (additional filtration may be necessary at this stage), which was stored in the glovebox over 4 Å molecular sieves. Alternatively, the product was also moderately stable when stored in the freezer outside the glovebox. It was noted that PhP(catechyl) can become malodorous with aging, though this does not compromise its reactivity. This reaction was sensitive to slight variations in experimental conditions. ^1H NMR (400 MHz, $CDCl_3$): δ (ppm) 7.62−7.56 (m, 2H), 7.48−7.35 (m, 3H), 7.18−7.11 (m, 2H), 7.03−6.97 (m, 2H). ^{13}C NMR (75 MHz, $CDCl_3$): δ (ppm) 146.5 (d, J_{CP} = 6.8 Hz), 141.7 (d, J_{CP} = 49.0 Hz), 131.7, 128.5 (d, J_{CP} = 22.6 Hz), 128.4 (d, J_{CP} = 5.1 Hz), 122.7 (d, J_{CP} = 0.5 Hz), 113.0 (d, J_{CP} = 0.8 Hz). ^{31}P NMR (81 MHz, $CDCl_3$): δ (ppm) 180.1. ^{31}P NMR (81 MHz, CD_2Cl_2): δ (ppm) 174.2. HRMS (ESI^+) for $C_{12}H_{10}O_2P^+$: calcd 217.04129, found 217.04192 (error m/z = 2.8 ppm).

Synthesis of (o-$O_2C_6H_4$)PF [FP(catechyl)]. To dry NaF (3.05 g, 50 mmol) in a 50 mL flask under nitrogen were added neat o-phenylene phosphorochloridite (2.38 mL, 20 mmol) and 15-crown-5 (0.40 mL, 2.0 mmol). The reaction is complete within 3 h. The product was very volatile and could be selectively distilled from the 15-crown-5 in the crude mixture by vacuum transfer; the crude was frozen ($N_{2\ (liq)}$) and placed under static high vacuum. It was allowed to warm to room temperature without additional heating with collection into a liquid nitrogen-cooled flask. The room-temperature product was obtained as an oil (1.76 g, 56% yield) with spectral properties consistent with the literature.[46] ^1H NMR (300 MHz, $CDCl_3$): δ (ppm) 7.26−7.19 (m, 2H), 7.15−7.05 (m, 2H). ^{13}C NMR (75 MHz, $CDCl_3$): δ (ppm) 143.8 (d, J_{CP} = 6.9 Hz), 123.7, 113.3. ^{31}P NMR (202 MHz, $CDCl_3$): δ (ppm) 124.7 (d, J_{PF} = 1306.6 Hz). ^{31}P NMR (81 MHz, CD_3CN): δ (ppm) 124.8 (d, J_{PF} = 1296.2 Hz).

Synthesis of 3a. In the glovebox, PhHC=NMe (1.19 g, 10.0 mmol) and benzoyl chloride (1.41 g, 10.0 mmol) were mixed in ca. 2 mL of acetonitrile and allowed to stand for 30 min. Triphenylphosphine (2.63 g, 10.0 mmol) was added as a CH_2Cl_2 (ca. 5 mL) solution. The solvent was removed in vacuo and the crude re-evaporated from THF and dissolved in THF (100 mL). Outside the glovebox, n-BuLi (4.1 mL, 10.3 mmol, as 2.5 M hexanes solution) was added dropwise at −78 °C. Stirring overnight at room temperature and concentration in vacuo yielded 4.0 g of solid product (82%). Crystallization conditions: In the glovebox, a benzene solution of **3a** (100 mg) was concentrated until viscous, partially precipitated with Et_2O, and gravity filtered through dry Celite. Et_2O was slowly diffused into the resulting saturated solution of **3a** using base bath, water, and acetone cleaned vials, yielding crystals suitable for X-ray analysis. ^1H NMR (400 MHz, $CDCl_3$): δ (ppm) 7.97−7.83 (very broad s, 2H), 7.60−6.85 (m, 20H), 6.73−6.50 (m, 3H), 3.28 (s, 3H). ^{13}C NMR (75.5 MHz, $CDCl_3$): δ (ppm) 176.1, 145.8 (d, $^1J_{C-P}$ = 28.7 Hz), 138.2, 133.9, 133.8, 132.2 (d, $^4J_{C-P}$ = 2.9 Hz), 129.1 (d, $^{2\ or\ 3}J_{C-P}$ = 12.0 Hz), 128.8 (d, J_{C-P} = 6.9 Hz), 128.4 (broad s), 127.3, 126.9, 118.7 (d, J_{C-P} = 6.6 Hz), 115.7, 56.2 (d, $^1J_{C-P}$ = 144.5 Hz), 39.6. ^{31}P NMR (81 MHz, $CDCl_3$): δ (ppm) 11.0. ^{31}P NMR (121 MHz, solid state): δ (ppm) 12.2. HRMS (ESI^+) for $C_{33}H_{29}NOP^+$: calcd 486.19813, found 486.19744 (error m/z = 1.4 ppm).

Synthesis of 2b. In the glovebox, PhHC=NMe (596 mg, 5.00 mmol) and benzoyl chloride (773 mg, 5.50 mmol) were mixed in ca. 1 mL acetonitrile and allowed to stand for 30 min. An acetonitrile solution (ca. 2 mL) of PhP(catechyl) (1.51 g, 7.00 mmol) was added followed by DBU (1.52 g, 10.0 mmol), and the mixture was diluted with acetonitrile to ca. 10 mL total volume and cooled at ca. − 40 °C overnight to improve product precipitation. Filtration, washing with cold acetonitrile, and removal of trace solvent residues in vacuo for ca. 12 h provides 1.76 g of product (80% yield). Crystallization conditions: In the glovebox, **2b** (100 mg) was partially precipitated from a dichloromethane solution (ca. 1 mL, 15 min dissolution time) by benzene addition. Gravity filtration through a ca. 0.5 cm pad of dry Celite (do not prewet with solvent), addition of a few drops of CH_2Cl_2, and slow evaporation from an uncapped 1 dram vial (cleaned with base bath, water, and acetone) undisturbed yielded needle crystals suitable for X-ray analysis. ^1H NMR (300 MHz, C_6D_6): δ (ppm) 8.01 (dd, J = 17, 8.1 Hz, 2H), 7.42 (d, J = 6.9 Hz, 2H), 7.29−7.19 (m, 2H), 7.17−7.00 (m, 6H), 6.95−6.80 (m, 4H), 6.60 (broad s, 3H), 2.56 (s, 3H). ^{13}C NMR

(42) Layer, R. *Chem. Rev.* **1963**, *63*, 489.
(43) (a) Becke, A. D. *J. Chem. Phys.* **1993**, *98*, 5648–5652. (b) Stephens, P. J.; Devlin, F. J.; Chabalowski, C. F.; Frisch, M. J. *J. Phys. Chem.* **1994**, *98*, 11623–11627. (c) Lee, C.; Yang, W.; Parr, R. G. *Phys. Rev. B* **1988**, *37*, 785–789.
(44) Gonzalez, C.; Schlegel, H. B. *J. Chem. Phys.* **1989**, *90*, 2154–2161.
(45) (a) Berlin, K. D.; Nagabhushanam, M. *J. Org. Chem.* **1964**, *29*, 2056. (b) Wieber, M.; Hoos, W. R. *Tetrahedron Lett.* **1968**, *51*, 5333. (c) Weiber, M.; Hoos, W. R. *Monatsh. Chem.* **1970**, *101*, 776.
(46) Farooq, O. *New J. Chem.* **2000**, *24*, 81.
(47) Padwa, A.; Haffmanns, G.; Tomas, M. *J. Org. Chem.* **1984**, *49*, 3314.

(75.5 MHz, DMSO-d_6): δ (ppm) 149.2, 148.1, 145.7, 143.1 (d, $^1J_{C-P}$ = 225.1 Hz), 136.4 (d, $^3J_{C-P}$ = 19.1 Hz), 134.6 (d, $^4J_{C-P}$ = 5.5 Hz), 130.9, 129.5, 128.8$_1$, 128.8$_0$ (d, $^{2\text{ or }3}J_{C-P}$ = 17.9 Hz), 128.2 (d, $^{2\text{ or }3}J_{C-P}$ = 11.5 Hz), 128.0, 126.6, 125.9, 122.6, 119.9, 111.3 (broad d, $^3J_{C-P}$ = 11.8 Hz), 110.8 (broad d, $^3J_{C-P}$ = 6.1 Hz), 76.2 (d, $^1J_{C-P}$ = 262.1 Hz), 38.1 (d, $^3J_{C-P}$ = 7.9 Hz). ^{31}P NMR (81 MHz, C_6D_6): δ (ppm) − 19.6. ^{31}P NMR (81 MHz, $CDCl_3$): δ (ppm) −18.9. ^{31}P NMR (121 MHz, solid state): δ (ppm) −22.2. HRMS (ESI$^+$) for $C_{27}H_{23}NO_3P^+$: calcd 440.14101, found 440.14096 (error m/z = 0.1 ppm).

X-ray Crystallographic Studies of 3a and 2b. X-ray crystallographic data were collected from a single-crystal sample, which was mounted on a loop fiber. Data were collected using a Bruker Platform diffractometer, equipped with a Bruker SMART 4K charged-coupled device (CCD) area detector using the program APEX2 and a Nonius FR591 rotating anode equipped with a Montel 200 optics. Upon isolation, the crystals were covered in paratone-N and placed under a 150 K N_2 stream on the goniometer head of a Bruker microstar area detector system (graphite-monochromated Cu KR radiation, λ = 1.54178 Å). The structures were solved by direct methods (SHELXL). All non-hydrogen atoms were refined anisotropically unless stated, and hydrogen atoms were treated as idealized contributions (Riding model).

General Procedure for PR_3 Screening (Table 1). In the glovebox, (4-$CH_3C_6H_4$)HC=$NCH_2C_6H_5$ (41.9 mg, 0.200 mmol) and *p*-methoxybenzoyl chloride (34.1 mg, 0.200 mmol) were mixed in ca. 0.1 mL of CD_2Cl_2, allowed to stand for 1 h, diluted to ca. 0.7 mL with CD_2Cl_2, and transferred into a septum-sealed NMR tube. Outside the glovebox, TMSOTf (36.3 μL, 0.200 mmol), phosphorus(III) reagent (0.200 mmol), and LiHMDS (0.22 mL, 0.22 mmol, 1.0 M hexanes solution, dropwise at −78 °C) were injected in order with inversion to promote mixing. Room-temperature ^{1}H and ^{31}P NMR data on **2/3** were obtained. The addition of dimethyl acetylenedicarboxylate (74 μL, 0.60 mmol) was immediately followed by ^{1}H NMR analysis, showing complete conversion in all reactive dipoles within 1−5 min. The pyrrole product was isolated by column chromatography (ethyl acetate/hexanes eluent).

Typical Procedure for Pyrrole Synthesis (Table 4, Entry 1). In the glovebox, (4-MeOPh)HC=N(CH_2CHCH_2) (88 mg, 0.50 mmol) and *p*-methoxybenzoyl chloride (85 mg, 0.50 mmol) were mixed in ca. 0.1 mL chloroform and allowed to stand for 30 min. PhP(catechyl) (162 mg, 0.75 mmol), DBU (152 mg, 1 mmol), and ethyl propiolate (147 mg, 1.5 mmol) were added in order as solutions in chloroform, bringing the final volume to 1 mL. The reaction is complete in many cases once all additions have been made. The solution was concentrated in vacuo followed by column chromatography (ethyl acetate/hexanes as eluent) to yield 165 mg of product (0.420 mmol, 84% yield). The pyrrole products are generally fluorescent blue spots with R_f ca. 0.2 on TLC with 5−30% ethyl acetate/hexanes as eluent. Pyrrole regioisomers were distinguished by a combination of NMR experiments (NOE, COSY, HMQC, HMBC at 2−3 then 4−5 bond setting).

Synthesis of Alkyl−Acid Chloride Derived Pyrroles (Table 4, Entry 6). In the glovebox, PhHC=N($CH_2C_6H_5$) (97.6 mg, 0.50 mmol) and isobutyryl chloride (53.3 mg, 0.50 mmol, 0.5 mL) were mixed in ca. 0.1 mL of CH_2Cl_2 and allowed to stand for 30 min. PhP(catechyl) (108 mg, 0.5 mmol) was added and the mixture diluted to ca. 0.7 mL final volume with CH_2Cl_2. Outside the glovebox, the mixture was cooled to −78 °C under nitrogen, and LiHMDS (500 μL, 0.5 mmol, 1.0 M solution in THF) was added dropwise. Methyl propiolate was injected (125 μL, 1.5 mmol), the cooling bath removed, and the mixture allowed to warm to rt over 0.5 h. The solution was concentrated in vacuo followed by column chromatography (ethyl acetate/hexanes eluent) to yield 113 mg product (0.339 mmol, 67% yield).

Synthesis of *C*-Alkyl Imine Derived Pyrroles (Table 4, Entry 9). To $(CH_3)_2CHHC$=$NCH_2C_6H_5$ (32.2 mg, 0.200 mmol) in dichloromethane (0.5 mL) under nitrogen at −78 °C was added *p*-toluoyl chloride (26 μL, 0.50 mmol) via syringe. The −78 °C bath was then replaced for a −15 °C bath (ethylene glycol/dry ice), and PhP(catechyl) (36 μL, 0.22 mmol, d = 1.34 g/mL) was injected, followed by AgOTf (51.4 mg, 0.200 mmol, acetonitrile solution). The mixture was warmed to room temperature and then recooled to −78 °C, and LiHMDS (200 μL, 0.20 mmol, 1.0 M solution in THF) was added dropwise. Dimethyl acetylenedicarboxylate was injected (98 μL, 0.8 mmol), and the mixture allowed to warm to rt over 0.5 h. The solution was concentrated in vacuo followed by column chromatography (ethyl acetate/hexanes as eluent) to yield 49.9 mg product (61% yield).

Pyrrole Regiochemistry. For pyrroles of Tables 3 and 4, entries 2−6, a series of 1D and 2D NOE NMR experiments were used to assign regiochemistry. For pyrroles of Table 3, entries 1, 2, and 4, and Table 4, entries 2−6, a correlation was observed between pyrrole C4-H and the adjacent aromatic substituent on C5. For pyrroles of Table 3, entries 3, 5, and 6, a correlation was observed between the methyl ester protons and adjacent aromatic group. See the Supporting Information for spectra.

Spectroscopic Data for Pyrroles. Table 3, Entry 1. Isolated yield: 89%. ^{1}H NMR (500 MHz, $CDCl_3$): δ (ppm) 7.26 (d, J = 6.5 Hz, 2H), 7.21 (d, J = 8.0 Hz, 2H), 7.19−7.11 (m, 5H), 6.88 (d, J = 6.5 Hz, 2H), 6.79 (s, 1H), 6.69−6.65 (m, 2H), 5.06 (s, 2H), 3.81 (s, 3H), 3.71 (s, 3H), 2.36 (s, 3H). ^{13}C NMR (125.7 MHz, $CDCl_3$): δ (ppm) 165.5, 159.8, 140.2, 138.6, 137.8, 135.3, 132.1, 130.0, 129.4$_5$, 129.4$_2$, 128.6, 127.3, 126.2, 124.3, 113.8, 113.6, 110.7, 55.4, 51.1, 48.6, 21.5. HRMS (ESI$^+$) for $C_{27}H_{26}NO_3^+$: calcd 412.19072, found 412.19040 (error m/z = 0.8 ppm). Anal. Calcd for $C_{27}H_{25}NO_3$: C, 78.81; H, 6.12; N, 3.40. Found: C, 78.47; H, 6.29; N, 3.35.

Table 3, Entry 2. Isolated yield: 92%. ^{1}H NMR (300 MHz, $CDCl_3$): δ (ppm) 7.30 (d, J = 9.0 Hz, 2H), 7.22−7.11 (m, 7H), 6.91 (d, J = 9.0 Hz, 2H), 6.70−6.61 (m, 2H), 6.54 (s, 1H), 5.13 (s, 2H), 3.81 (s, 3H), 2.35 (s, 3H). ^{13}C NMR (75 MHz, $CDCl_3$): δ (ppm) 160.1, 142.5, 138.1, 137.7, 136.3, 131.0, 129.2, 128.6, 128.5, 127.3, 125.7, 121.9, 117.4, 114.2, 111.5, 92.8, 55.2, 48.8, 21.2. HRMS (ESI$^+$) for $C_{26}H_{22}N_2O^+$: calcd 379.18049, found 379.18019 (error m/z = 0.8 ppm).

Table 3, Entry 3. Isolated yield: 52%. ^{1}H NMR (500 MHz, $CDCl_3$): δ (ppm) 7.20−7.07 (m, 9H), 6.85 (d, J = 8.5 Hz, 2H), 6.62−6.66 (m, 2H), 4.88 (s, 2H), 3.81 (s, 3H), 3.64 (s, 3H), 2.36 (s, 3H), 2.24 (s, 3H). ^{13}C NMR (125 MHz, $CDCl_3$): δ (ppm) 166.2, 159.2, 138.9, 138.4, 137.4, 132.3, 131.7, 130.8, 128.9, 128.1, 126.7, 125.9, 124.8, 118.6, 113.2, 112.7, 55.1, 50.4, 48.2, 21.2, 11.8. HRMS (ESI$^+$) for $C_{28}H_{28}NO_3^+$: calcd 426.20637, found: 426.20605 (error m/z = 0.8 ppm).

Table 3, Entry 4. Isolated yield: 92%. ^{1}H NMR (500 MHz, $CDCl_3$): δ (ppm) 7.31−7.17 (m, 2H), 7.23−7.13 (m, 7H), 6.84 (d, J = 8.5 Hz, 2H), 6.68−6.60 (m, 2H), 6.51 (s, 1H), 5.11 (s, 2H), 2.80 (s, 3H), 2.36 (s, 3H). ^{13}C NMR (75 MHz, $CDCl_3$): δ (ppm) 159.5, 142.5, 139.0, 137.6, 136.0, 130.7, 129.4$_4$, 129.4$_3$, 128.4, 127.2, 126.7, 125.7, 123.8, 117.4, 113.9, 111.5, 92.7, 55.2, 48.8, 21.2. HRMS (ESI$^+$) for $C_{26}H_{22}N_2O^+$: calcd 379.18049, found 379.18024 (error m/z = 0.7 ppm).

Table 3, Entry 5. Isolated yield: 91%. ^{1}H NMR (400 MHz, $CDCl_3$): δ (ppm) 7.24 (d, J = 8.4 Hz, 2H), 7.20−7.10 (m, 7H), 6.86 (d, J = 7.6 Hz, 2H), 6.74 (s, 1H), 6.69−6.61 (m, 2H), 5.02 (s, 2H), 3.80 (s, 3H), 3.70 (s, 3H), 2.36 (s, 3H). ^{13}C NMR (125.7 MHz, $CDCl_3$): δ (ppm) 165.5, 159.5, 140.2, 138.6, 138.3, 135.0, 130.9, 130.7, 129.1, 128.9, 128.5, 127.2, 126.1, 125.3, 114.1, 113.6, 110.5, 55.5, 51.1, 48.6, 21.6. HRMS (ESI$^+$) for $C_{27}H_{26}NO_3^+$: calcd 412.19072, found 412.19030 (error m/z = 1.0 ppm).

Table 3, Entry 6. Isolated yield: 47%. ^{1}H NMR (500 MHz, $CDCl_3$): δ (ppm) 7.21−7.08 (m, 9H), 6.86 (d, J = 8.0 Hz, 2H), 6.63−6.55 (m, 2H), 4.87 (s, 2H), 3.80 (s, 3H), 3.64 (s, 3H), 2.36 (s, 3H), 2.23 (s, 3H). ^{13}C NMR (125 MHz, $CDCl_3$): δ (ppm) 166.2, 159.0, 139.0, 138.3, 137.6, 132.2, 132.0, 130.4, 129.6, 128.5, 128.0, 126.7, 125.9, 124.1, 118.7, 113.6, 112.5, 55.1, 50.4, 48.1, 21.3, 11.7. HRMS (ESI$^+$) for $C_{28}H_{28}NO_3^+$: calcd 426.20637, found 426.20627 (error m/z = 0.2 ppm).

Table 4, Entry 1. Isolated yield: 84%. ^{1}H NMR (400 MHz, $CDCl_3$): δ (ppm) 7.37 (d, J = 8.8 Hz, 2H), 7.33 (d, J = 8.8 Hz, 2H), 7.00−6.90 (m, 4H), 6.68 (s, 1H), 5.66−5.54 (m, 1H), 5.02 (d, J = 10.4 Hz, 1H), 4,66 (d, J = 17,2 Hz, 1H), 4.42−4.32 (m, 2H), 4.13 (q, J = 7.2, 2H), 3.84$_6$ (s, 3H), 3.83$_8$ (s, 3H), 1.16 (t, J = 6.8, 3H). ^{13}C NMR (75.5 MHz, $CDCl_3$): δ (ppm) 165.1, 159.8, 159.5, 139.3, 134.7, 134.5, 132.2, 130.9, 125.5, 124.7, 116.6, 114.0, 113.8, 113.5, 110.2, 59.5, 55.5, 55.4, 47.2, 14.5. HRMS (ESI$^+$) for $C_{24}H_{26}NO_4^+$: calcd 392.18564, found 392.18520 (error m/z = 1.1 ppm).

Table 4, Entry 2. Isolated yield: 89%. ^{1}H NMR (500 MHz, $CDCl_3$): δ (ppm) 7.38−7.26 (m, 4H), 7.21 (d, J = 7.0 Hz, 2H), 6.95 (d, J = 8.0 Hz, 2H), 6.69 (s, 1H), 5.65−5.55 (m, 1H), 5.01 (d, J = 10.0, 1H), 4.65 (d, J = 17.5 Hz, 1H), 4.39 (s, 2H), 3.85 (s, 3H), 3.68 (s, 3H), 2.39 (s, 3H). ^{13}C NMR (125.7 MHz, $CDCl_3$): δ (ppm) 165.5, 159.9, 139.8, 137.8, 134.8, 134.7, 132.2, 130.1, 129.4$_5$, 129.3$_6$, 124.4, 116.7, 113.6, 113.4, 110.3, 55.4, 51.0, 47.2, 21.5. HRMS (ESI$^+$) for $C_{23}H_{24}NO_3^+$: calcd 362.17507, found 362.17471 (error m/z = 1.0 ppm).

Table 4, Entry 3. Isolated yield: 90%. ^{1}H NMR (400 MHz, $CDCl_3$): δ (ppm) 7.38 (d, J = 8.4 Hz, 2H), 7.30 (d, J = 8.0 Hz, 2H), 7.24 (d, J = 7.6 Hz, 2H), 6.95 (d, J = 8.4 Hz, 2H), 6.69 (s, 1H), 5.68−5.55 (m, 1H), 5.03 (d, J = 10.4 Hz, 1H), 4.67 (d, J = 17.2 Hz, 1H), 4.39 (s, 2H), 3.85 (s, 3H), 3.69 (s, 3H), 2.42 (s, 3H). ^{13}C NMR (100.6 MHz, $CDCl_3$): δ (ppm) 165.2, 159.3, 139.6, 138.2, 134.4$_4$, 134.3$_8$, 130.7, 130.5, 129.1, 128.7, 125.1, 116.4, 113.8, 113.0, 109.9, 55.3, 50.8, 46.9, 21.5. HRMS (ESI$^+$) for $C_{23}H_{24}NO_3^+$: calcd 362.17507, found 362.17487 (error m/z = 0.6 ppm).

Table 4, Entry 4. Isolated yield: 74%. ^{1}H NMR (300 MHz, $CDCl_3$): δ (ppm) 7.53 (s, 1H), 7.42−7.31 (m, 2H), 7.16−7.04 (m, 2H), 6.87 (d, J = 3.4 Hz, 1H), 6.54−6.50 (m, ^{1}H), 6.48 (s, 1H), 5.92−5.76 (m, 1H), 5.14 (d, J = 10.6 Hz, 1H), 4,79 (d, J = 17.3 Hz, 1H), 4.72−4.63 (m, 2H). ^{13}C NMR (75.5 MHz, $CDCl_3$): δ (ppm) 164.7, 161.4, 143.8, 143.0, 136.0, 133.8, 131.6, 131.5, 127.3$_0$, 127.2$_6$, 117.1, 117.0, 116.1, 115.8, 112.5, 111.9, 111.1, 92.4, 48.8. HRMS (ESI$^+$) for $C_{18}H_{14}FN_2O^+$: calcd 293.10846, found 293.1091 (error m/z = 2.0 ppm).

Table 4, Entry 5. Isolated yield: 69%. ^{1}H NMR (500 MHz, $CDCl_3$): δ (ppm) 7.42−7.34 (m, 3H), 7.30 (d, J = 7.5 Hz, 2H), 7.15−7.09 (m, 2H), 6.58 (s, 1H), 4.05 (q, J = 7.5 Hz, 2H), 2.42 (s, 3H), 1.03 (t, J = 7.4 Hz). ^{13}C NMR (125 MHz, $CDCl_3$): δ (ppm) 142.5, 139.3, 132.4, 129.6, 129.5, 127.5, 127.4, 127.3, 126.7, 126.5, 117.0, 113.3, 92.8, 40.4, 21.3, 16.2. HRMS (ESI$^+$) for $C_{18}H_{17}N_2S^+$: calcd 293.11070, found 293.11030 (error m/z = 1.3 ppm).

Table 4, Entry 6. Isolated yield: 67%. ^{1}H NMR (400 MHz, $CDCl_3$): δ (ppm) 7.35−7.22 (m, 8H), 6.93 (d, J = 7.2 Hz, 2H), 6.72 (s, 1H), 5.19 (s, 2H), 3.83 (s, 3H), 3.25−3.13 (m, 1H), 1.29 (d, J = 7.2 Hz, 6H). ^{13}C NMR (100 MHz, $CDCl_3$): δ (ppm) 165.3, 146.2, 138.4, 133.6, 132.7, 129.3, 128.8, 128.4, 127.6, 127.3, 125.5, 111.6, 111.4, 50.9, 48.3, 26.7, 20.1. HRMS (ESI$^+$) for $C_{22}H_{24}NO_2^+$: calcd 334.18016, found 334.17984 (error m/z = 1.0 ppm). Anal. Calcd for $C_{22}H_{23}NO_2$: C, 79.25; H, 6.95; N, 4.20. Found: C, 79.12; H, 7.18; N, 4.07.

Table 4, Entry 7. Isolated yield: 24%. ^{1}H NMR (500 MHz, $CDCl_3$): δ (ppm) 7.36 (d, J = 8.0 Hz, 2H), 7.32−7.00 (m, 6H), 6.30 (s, 1H), 4.92 (s, 2H), 3.97 (q, J = 7.5 Hz, 2H), 2.42 (s, 3H), 2.41 (s, 3H), 2.34 (q, J = 7.5 Hz, 2H), 1.14 (t, J = 7.5 Hz, 3H), 0.87 (t, 3H, J = 7.0 Hz). ^{13}C NMR (125 MHz, $CDCl_3$): δ (ppm) 174.7, 137.6, 136.8, 134.4, 130.7$_6$, 130.7$_4$, 130.5, 129.1, 129.0, 116.3, 116.2, 109.8, 60.0$_8$, 60.0$_6$, 39.7, 27.7, 21.2$_4$, 21.1$_7$, 16.2, 9.1. HRMS (ESI$^+$) for $C_{24}H_{27}NO_2Na^+$: calcd 384.19340, found 384.19341 (error m/z = 0.1 ppm).

Table 4, Entries 8 and 9. Isolated yields: 83 and 61%, respectively. ^{1}H NMR (400 MHz, $CDCl_3$): δ (ppm) 7.32−7.20 (m, 3H), 7.18−7.07 (m, 4H), 6.86 (d, J = 7.2 Hz, 2H), 4.97 (s, 2H), 3.86 (s, 3H), 3.62 (s, 3H), 3.02−2.90 (m, 1H), 2.32 (s, 3H), 1.20 (d, J = 7.2 Hz, 6H). ^{13}C NMR (75 MHz, $CDCl_3$): δ (ppm) 167.6, 165.3, 140.6, 138.7, 137.7, 136.9, 130.6, 129.1, 129.0, 128.1, 127.7, 125.7, 113.8, 113.4, 52.1, 51.6, 48.0, 26.7, 21.5$_9$, 21.5$_5$. HRMS (ESI$^+$) for $C_{25}H_{28}NO_4^+$: calcd 406.20129, found 406.20093 (error m/z = 0.9 ppm).

Table 4, Entry 10. Isolated yield: 44%. ^{1}H NMR (400 MHz, $CDCl_3$): δ (ppm) 7.42−7.33 (m, 3H), 7.32−7.23 (m, 6H), 6.98−6.92 (m, 2H), 4.93 (m, 2H), 3.81 (m, 3H), 3.67 (m, 3H). ^{13}C NMR (125 MHz, $CDCl_3$): δ (ppm) 165.5, 164.1, 137.3, 136.3, 130.4, 130.0, 128.8, 128.3, 128.0, 127.0, 126.9, 115.5, 115.0, 51.7, 51.5, 51.2. HRMS (ESI$^+$) for $C_{21}H_{20}NO_4^+$: calcd 350.13869, found 350.13827 (error m/z = 1.2 ppm).

Table 4, Entry 11. Isolated yield: 30%. ^{1}H NMR (300 MHz, $CDCl_3$): δ (ppm) 8.55 (d, J = 7.9 Hz, 1H), 7.59−7.49 (m, 3H), 7.48−7.42 (m, 1H), 7.42−7.35 (m, 2H), 7.07−7.00 (m, 2H), 6.79 (d, J = 7.4 Hz, 1H), 4.02 (s, 3H), 3.88 (s, 3H), 3.72 (s, 3H). ^{13}C NMR (75.5 MHz, $CDCl_3$): δ (ppm) 168.0, 165.3, 160.5, 132.5, 129.8, 128.5, 128.4, 128.2, 127.8, 127.4, 125.5, 124.5, 121.9, 121.5, 117.1, 114.4, 114.2, 109.2, 52.6, 52.8, 52.0. HRMS for $C_{23}H_{20}NO_5^+$: calcd 390.13360, found 390.13434 (error m/z = 1.9 ppm).

Table 4, Entry 12. Isolated yield: 60%. ^{1}H NMR (400 MHz, $CDCl_3$): δ (ppm) 7.54 (d, J = 7.6 Hz, 2H), 7.40−7.10 (m, 11H), 7.05−6.95 (m, 2H), 6.93−6.80 (m, 4H), 5.26 (s, 2H). ^{13}C NMR (75.5 MHz, $CDCl_3$): δ (ppm) 192.0, 139.2, 137.8, 136.1, 132.3, 131.4, 130.1, 130.0, 129.2, 128.9, 128.5, 128.1, 127.7, 127.1, 126.1, 49.1. HRMS (ESI$^+$) for $C_{32}H_{20}NO_7^+$: calcd 530.12343, found 530.12378 (error m/z = 0.7 ppm).

Table 4, Entry 13. Isolated yield: 32%. ^{1}H NMR (300 MHz, $CDCl_3$): δ (ppm) 7.48 (s, 1H), 7.44−7.35 (m, 2H), 7.18−7.07 (m, 2H), 6.51−6.46 (m, 2H), 6.44−6.40 (m, 1H), 6.19 (d, J = 3.3 Hz, 1H), 4.14 (q, J = 7.2 Hz, 2H), 1.162 (t, J = 7.2 Hz, 3H). ^{13}C NMR (125 MHz, $CDCl_3$): δ (ppm) 162.2 (d, $^1J_{C-F}$ = 246.9 Hz), 147.9, 141.4, 134.9, 131.0 (d, $^2J_{C-F}$ = 7.9 Hz), 129.6 (d, $^4J_{C-F}$ = 3.4 Hz), 125.0, 115.3 (d, $^3J_{C-F}$ = 21.5 Hz), 111.1, 109.4, 109.3, 106.3, 40.2, 16.4. HRMS (ESI$^+$) for $C_{16}H_{15}NOF^+$: calcd 256.11322, found 256.11293 (error m/z = 1.1 ppm).

Table 4, Entry 14. Isolated yield: 42%. ^{1}H NMR (500 MHz, $CDCl_3$): δ (ppm) 7.22−7.07 (m, 5H), 7.04−6.93 (m, 6H), 6.77 (d, J = 9.0 Hz, 2H), 6.47 (s, 1H), 6.45 (s, 1H), 3.79 (s, 3H), 2.30 (s, 3H). ^{13}C NMR (125 MHz, $CDCl_3$): δ (ppm) 158.4, 136.0, 135.8, 135.6, 133.7, 132.0, 130.4, 129.8, 128.6$_2$, 128.5$_6$, 127.8, 126.0, 113.9, 109.5, 109.3, 55.3, 21.0. HRMS (ESI$^+$) for $C_{24}H_{22}NO^+$: calcd 340.16959, found 340.16952 (error m/z = 0.2 ppm). Note: rapid H−D exchange in $CDCl_3$ yielded extra carbon and MS signals. ^{13}C NMR (125 MHz, $CDCl_3$): δ (ppm) 135.9, 135.5, 109.4, 109.2. HRMS (ESI$^+$) for $C_{24}H_{21}DNO^+$: calcd 341.17587, found 341.17587 (error m/z = 0.0 ppm).

Table 4, Entry 15. Isolated yield: 35%. ^{1}H NMR (500 MHz, $CDCl_3$): δ (ppm) 7.99 (s, 1H), 7.97−7.91 (m, 3H), 7.68 (d, J = 8.0 Hz, 1H), 7.64−7.46 (m, 6H), 7.43−7.36 (m, 1H), 6.45 (s, 1H), 6.39 (s, 1H), 4.25 (q, 2H, J = 7.0 Hz), 0.91 (t, 3H, J = 7.0 Hz). ^{13}C NMR (125 MHz, $CDCl_3$): δ (ppm) 136.3, 135.9, 134.0, 133.4, 132.3, 131.5, 129.0, 128.4, 127.9$_5$, 127.9$_4$, 127.7, 127.4, 127.3, 127.0, 126.3, 125.8, 110.1, 109.7, 40.1, 16.1. HRMS (ESI$^+$) for $C_{22}H_{20}N^+$: calcd 298.15903, found 298.15869 (error m/z = 1.1 ppm). Note: rapid H−D exchange in $CDCl_3$ yielded extra carbon and MS signals. ^{13}C NMR (125 MHz, $CDCl_3$): δ (ppm) 136.2, 135.8, 110.0, 109.6. HRMS (ESI$^+$) for $C_{22}H_{19}DN^+$: calcd 299.16530, found 299.16490 (error m/z = 1.3 ppm).

Table 4, Entry 16. Isolated yield: 63%. ^{1}H NMR (300 MHz, $CDCl_3$): δ (ppm) 7.23−7.13 (m, 3H), 6.89 (d, J = 8.4 Hz, 2H), 6.66 (d, J = 6.9 Hz, 2H), 6.52 (d, J = 8.7 Hz, 2H), 5.21 (s, 2H),

3.89 (s, 3H), 3.56 (s, 3H), 2.89 (s, 6H), 1.34 (s, 9H). ^{13}C NMR (75 MHz, $CDCl_3$): δ (ppm) 170.0, 164.0, 149.9, 141.0, 138.6, 137.1, 131.0, 128.1, 126.7, 125.3, 118.5, 115.4, 111.4, 111.1, 52.1, 50.8, 49.6, 40.0, 33.6, 30.6. HRMS (ESI^+) for $C_{27}H_{33}N_2O_4^+$: calcd 449.24348, found 449.24374 (error m/z = 0.6 ppm).

Acknowledgment. We thank the NSF, NSERC, FQRNT, DuPont, the CFI, and the Australian−American Fulbright Commission for financial support and the NCSA, UCLA ATS, and UCLA IDRE for computer resources. We also thank Warren Powell for assistance with the IUPAC name of the phospha-Münchnones **2** reported in the previous communication of this work.

Supporting Information Available: CIF files for **3a** and **2b**, NMR spectra of products, and B3LYP/6-31+G(d) geometries. This material is available free of charge via the Internet at http://pubs.acs.org.